

# From weak to strong-coupling superconductivity tuned by substrate in TiN films

Yixin Liu,<sup>1,2</sup> Zulei Xu,<sup>1,2</sup> Aobo Yu,<sup>1,2</sup> Xiaoni Wang,<sup>1,2</sup> Wei Peng,<sup>1,2</sup> Yu Wu,<sup>1,\*</sup> Gang Mu,<sup>1,2,†</sup> and Zhi-Rong Lin<sup>1,2,‡</sup>

<sup>1</sup>*National Key Laboratory of Materials for Integrated Circuits,  
Shanghai Institute of Microsystem and Information Technology,  
Chinese Academy of Sciences, Shanghai 200050, China*

<sup>2</sup>*University of Chinese Academy of Sciences, Beijing 100049, China*

The interplay between substrates and superconducting thin films has attracted increasing attention. Here, we report an in-depth investigation on superconducting properties of the epitaxial TiN thin films grown on two different substrates by dc reactive magnetron sputtering. The TiN films grown on (0001) sapphire exhibit (111) crystal orientation, while that grown on (100) Si substrates exhibit (100) orientation. Moreover, the samples grown on Si reveal a relatively lower level of disorder, accompanied by the higher critical transition temperature  $T_c$  and smaller magnitude of upper critical field slope near  $T_c$ . Remarkably, we uncovered a rather high value of superconducting gap (with  $\Delta_0/k_B T_c = 3.05$ ) in TiN film on Si indicating a very strong coupling superconductivity, in sharp contrast to the case using sapphires as the substrate which reveals a weak-coupling feature. Further analysis shows that the weakened electronic screening effect due to the high level of disorder and the suppressed electronic density of states may be the underlying reasons for the occurrence of weak coupling superconductivity in the TiN films based on sapphire substrate.

Keywords: strong coupling, TiN, superconducting gap, point-contact spectroscopy

## INTRODUCTION

Nitride superconducting thin films have excellent application performance in superconducting (SC) electronic device [1–4]. Due to the low microwave loss [5] and high kinetic inductance [6], TiN films attracted more and more interests for the application in superconducting microwave resonators [7–10] in recent years. It is reported that quality factor higher than  $2 \times 10^6$  can be achieved in microwave resonator made with TiN films [10, 11]. Typically TiN films can be grown by magnetron sputtering [12], pulsed laser deposition (PLD) [13, 14], and molecular beam epitaxy [15]. It is found that physical performance of TiN films can be tuned by the growth conditions like the chamber pressure and gas-flow rate [9]. The  $T_c$  value of TiN films grown on (100) MgO could be over 5 K, which is very close to bulk material [15].

The physical properties of TiN thin films have also been widely studied. The magnetic field induced superconductor-insulator transition has been observed in TiN thin films [16, 17]. Vortex matching effect was studied in nanoperforated ultrathin TiN films [18]. The emergence of ferromagnetism has been discovered in TiN with an increase in nitrogen vacancies [19]. Superconducting energy gap is an important parameter for superconducting materials, which can supply valuable information both for the physical understanding and the application of the materials. This issue has been investigated through scanning tunneling spectroscopy (STS) [20, 21] and tunneling junctions [22]. A strong spatial inhomogeneity with the gap value varying by a factor of 2 was found in TiN film [21]. The importance of interaction between the SC films and substrates was noticed in recent years [23–

26]. Specific to the TiN thin film, it was found that type of substrates has a clear impact on the lattice orientations, e.g., (111) TiN on *c*-cut sapphire [27–29], (110) TiN on *R*-plane sapphire [9], and (100) TiN on (100) magnesium oxide (MgO) [15] and (100) silicon [5, 13]. Meanwhile, disorder is another noteworthy factor, which can have a pronounced effect on the superconductivity in thin films [30]. At present, there is still a lack of comprehensive research on the superconducting behavior, especially in terms of superconducting gap, of TiN films with the variation of disorder level and crystal orientation.

In this work, we carried out the investigations on superconducting properties, especially superconducting gap, of TiN films grown on different substrates. It is found that the type of substrate has had a significant impact on both the crystal orientation and superconducting properties of TiN films. Importantly, the TiN film grown on (100) silicon substrate displays a significantly large superconducting gap which exceeds the prediction of weak-coupling BCS theory, while that on (0001) sapphire reveals a weak-coupling behavior. The analysis combining the Hall resistivity data indicates that the weakened electronic screening effect and the suppressed electronic density of states are responsible for the weak coupling in the sapphire-based TiN films.

## EXPERIMENTAL

TiN films were grown using dc magnetron sputtering equipped with a high vacuum pump. Two different substrates, (0001) sapphire (abbreviate as sapphire hereafter) and high resistivity (100) silicon (abbreviate as Si hereafter), were used. The sputtering process was

TABLE I: Summary of the information for the film growth and orientation.

Name	Substrate	Growth temperature	Film orientation
Sapp-310	Sapphire	310 °C	(111)
Sapp-500	Sapphire	500 °C	(111)
Si-500	Si	500 °C	(100)

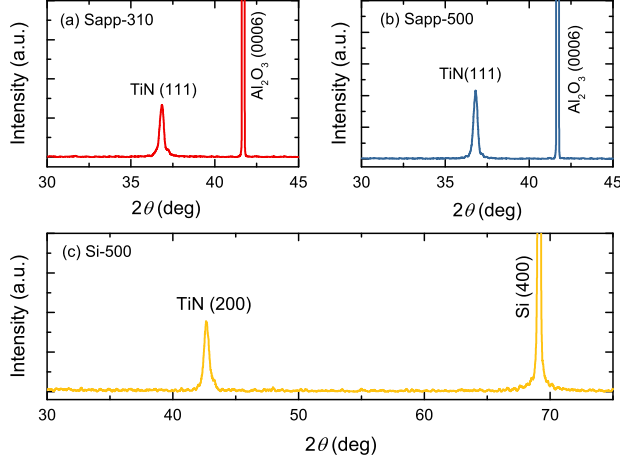


FIG. 1: XRD patterns of the three TiN films Sapp-310 (a), Sapp-500 (b), and Si-500 (c).

carried out in a mixed atmosphere of Ar (99.999%) and N<sub>2</sub> (99.999%). For the case that sapphire was used, two different growth temperatures, 310 °C and 500 °C, were adopted. With the Si substrate, TiN films were grown at 500 °C. The film thickness is 35 nm for all the samples. The detailed growth processes will be reported elsewhere. The information for the samples studied in this work are summarized in Table 1.

The crystal structures of films were measured by X-Ray diffraction (XRD, Bruker D8 Discover). The electrical transport measurement were performed on a physical property measurement system (PPMS, Quantum Design). The applied electric current is 10  $\mu$ A. The superconducting gap of TiN films were studied by point-contact spectroscopy. The point contact is achieved through the nano-Au array on the films. The nano-Au array was synthesized on film by using thermal evaporation through a nanoporous AAO mask attaching to the surface of TiN film. The commercially purchased AAO films were chosen to be the mask of the nano-Au array. The pore diameter of AAO film is 30 nm with the interpore distance of 60 nm and the thickness of 100 nm. The detailed processes for the fabrication of nano-Au array can be seen in our previous work [31].

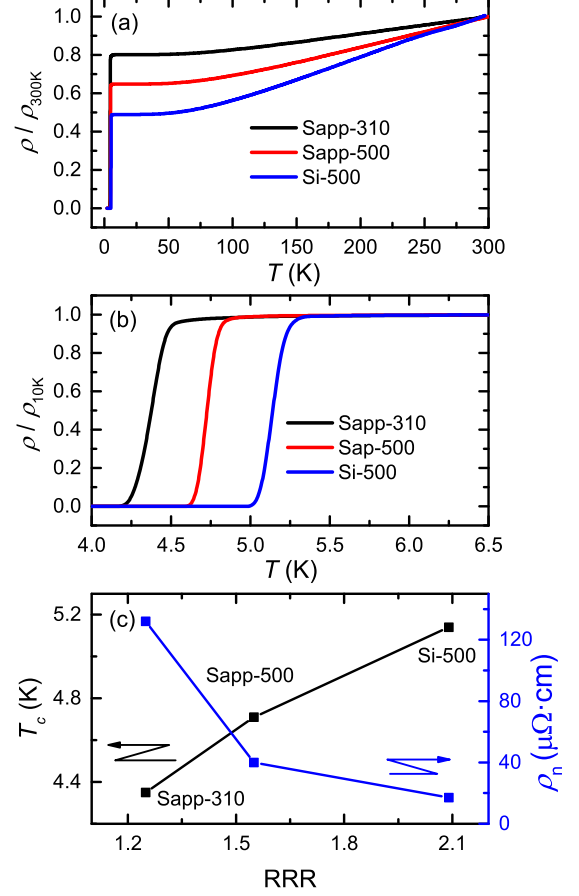


FIG. 2: (a) Normalized resistivity of the three samples as a function of temperature under zero magnetic field. (b) An enlarged view of the normalized resistivity data in the low temperature. (c) SC critical temperature  $T_c$  (left) and normal-state resistivity  $\rho_n$  (right) as a function of the residual resistivity ratio (RRR).

## RESULTS

The crystal structure of the films were checked by XRD. Figs. 1(a, b) show the XRD patterns of the two films grown on sapphire at different temperatures. The peaks at around 36.8 ° can be assigned to the (111) diffraction peaks of TiN. No peaks from other orientations can be detected, indicating the oriented growth of the films. For the film Si-500, only the (200) peak can be seen, see Fig. 1(c). Such substrate dependent film orientation is consistent with the previous report of other groups [5, 13, 27–29]. To have a quantitative comparison, we calculate the lattice constant of three films using the Bragg's Law. The lattice parameters vary very little among these three sample, ranging from 4.22 Å to 4.24 Å.

Normalized resistivity of the three samples is shown in

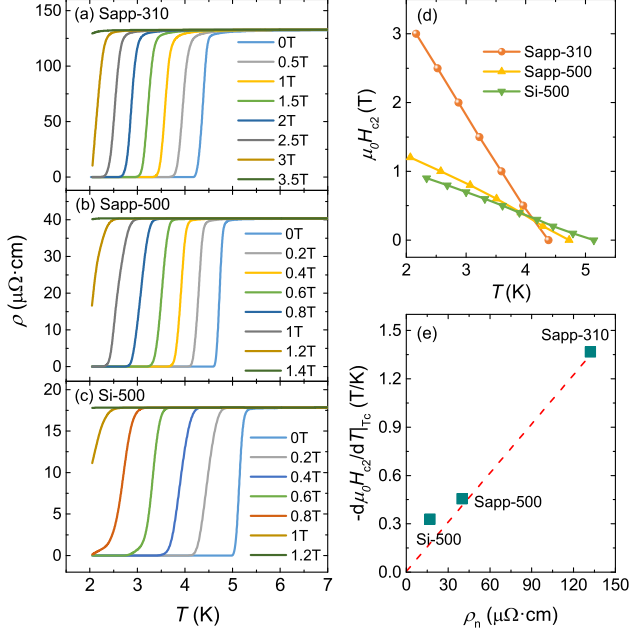


FIG. 3: (a-c) Temperature dependence of resistivity of the three samples under the magnetic field. (d) Upper critical fields  $\mu_0 H_{c2}$  as a function of temperature for the three samples. (e) Upper critical field slope near  $T_c$  as a function of  $\rho_n$ . The red dashed line is a guide for eyes.

Fig. 2(a). All the three samples reveal the SC transition in the low temperature region. The residual values of  $\rho/\rho_{300K}$  show a systematic evolution with the growth temperature  $T_{gr}$  and the type of substrate. In general, the residual resistivity ratio (RRR =  $\rho_{300K}/\rho_{10K}$ ) reflects the level of disorder in the film, which contributes a temperature-independent term to the electrical transport. Thus the data indicates that a higher value of  $T_{gr}$  can reduce the disorder level. Moreover, at the same growth temperature of 500 °C, sample on Si substrate shows a even low disorder level as represented by the larger value of RRR. The SC transition can be seen more clearly in the enlarged view in Fig. 2(b). The SC critical temperature  $T_c$  displays a similar tendency to RRR with the variation of  $T_{gr}$  and substrate. In the sample Si-500,  $T_c$  can be as high as 5.14 K determined using the standard of  $50\%\rho_n$ . Here  $\rho_n$  is the normal-state resistivity at the temperature just above the SC transition. In Fig. 2(c), we summarize the values of  $T_c$  and  $\rho_n$  as a function of RRR. It is evident that  $T_c$  is positively correlated with RRR, while  $\rho_n$  reveals a reverse evolution tendency. We note that this is a common feature in SC films [32, 33], which actually reflects the suppression effect on superconductivity in low dimension induced by disorder.

In Figs. 3(a-c), we show temperature-dependent resistivity with various magnetic fields perpendicular to the film surface for the three samples. As the field in-

creases, the SC transition shifts to lower temperatures. It is notable that the suppression efficiency of magnetic field on superconductivity shows significant differences among these three samples. For the sample Sapp-310 with the lowest  $T_c$ , superconductivity can survive under the field up to 3 T in the temperature range above 2 K. In contrast, superconductivity is suppressed completely by the field of 1.2 T for the sample Si-500 with a higher  $T_c$ . Such a comparison can be seen more clearly in Fig. 3(d), where the upper critical fields  $\mu_0 H_{c2}$  for all the three samples as a function of temperature are shown. In the temperature range above 2 K,  $\mu_0 H_{c2}$  display a linear decrease with the increase of temperature. The slope of this tendency,  $d\mu_0 H_{c2}/dT|_{T_c}$ , is plotted in Fig. 3(e) as a function of  $\rho_n$ . The roughly linear dependence of  $d\mu_0 H_{c2}/dT|_{T_c}$  with  $\rho_n$ , as represented by the red dashed line, actually accords with the expectations for dirty-limit superconductors [34].

The point-contact tunneling spectra of samples Sapp-500 and Si-500 at a wide temperatures range down to 0.1 K are shown in Figs. 4(a) and (c). The data are normalized to the spectrum at high temperatures where the superconductivity vanishes. Clear SC coherence peaks can be observed at low temperature region in both samples. As the temperature increases, the broadening effect becomes apparent, and the differential conductivity curves gradually become flat. The differential conductance spectra are analyzed using the Blonder-Tinkham-Klapwijk (BTK) theory [35]. The fitting results for the two samples at the lowest temperature  $T = 0.1$  K are shown in Figs. 4(b) and (d). For sample Si-500, in order to fit the data well, a term that remains constant with bias voltage is introduced. This may be due to the paralleling of other components in the point contacts. The obtained SC gaps are  $\Delta = 0.71$  meV and 1.35 meV for samples Sapp-500 and Si-500 respectively. Meanwhile, the broadening parameters for the two samples are  $\Gamma = 0.05$  meV and 0.18 meV respectively. The temperature dependence of gap values is summarized in Fig. 4(e), which is consistent with the BCS relation (see the solid lines). We note that although the  $T_c$  of sample Si-500 is slightly higher than that of Sapp-500, its SC gap value is significantly higher than the later.

To make a quantitative comparison, we plot the ratio  $\Delta_0/k_B T_c$  of three samples as a function of  $T_c$  in Fig. 4(f). Here  $\Delta_0$  is the extrapolated gap value in zero temperature, and  $k_B$  is the Boltzmann constant. It is found that the  $\Delta_0/k_B T_c$  value of Sapp-310 is slightly lower than the weak-coupling BCS prediction of 1.76, while that of Sapp-500 is very close to this value. Impressively, sample Si-500 exhibits a  $\Delta_0/k_B T_c$  value as high as 3.05. Our result reveals an evolution from weak- to strong-coupling superconductivity in TiN films by changing the substrate from sapphire to Si.

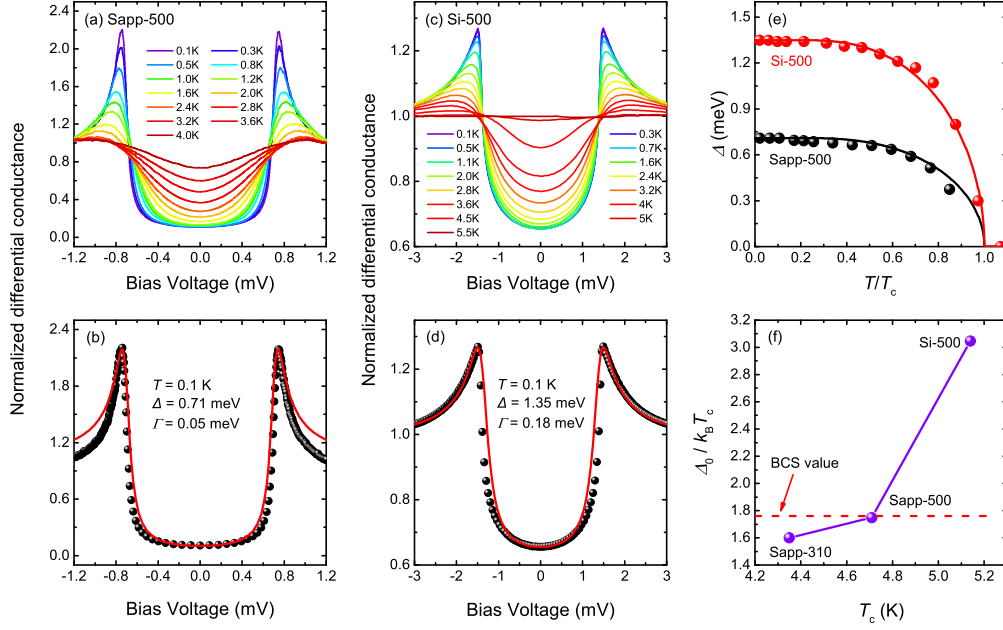


FIG. 4: (a, c) Temperature dependence of tunneling spectra of samples Sapp-500 and Si-500 respectively. (b, d) The spectrum data of the two samples at 0.1 K (black solid circles) with the best fitting result (red lines) using the BTK model. (e) Temperature dependence of the superconducting energy gap for the two samples. (f) The ratio  $\Delta_0/k_B T_c$  as a function of  $T_c$  for the three samples Sapp-310, Sapp-500, and Si-500. The red dashed line shows the value predicted by the BCS theory.

TABLE II: Experimental results about the SC gap in TiN and NbN films.

Sample	Substrate	$\Delta_0$ (meV)	$\Delta_0/k_B T_c$	Ref.
TiN	Si <sup>a</sup>	0.73	1.81	[20]
TiN	SiN/MgO <sup>b</sup>	0.83	2.4	[22]
TiN	Si	0.2-1.1	0.49-2.71	[21]
NbN <sup>c</sup>	MgO	1.47-2.80	1.95-2.22	[36]
TiN	Sapphire	0.60-0.71	1.60-1.75	This work
TiN	Si	1.35	3.05	This work

<sup>a</sup> The Si substrate was thermally oxidized. <sup>b</sup> The specific type of substrate is not explicitly stated in the paper. <sup>c</sup>  $T_c$  of NbN films covers a large range from 7.7 to 14.9 K.

## DISCUSSION

The SC gap of TiN films have also been studied by other groups. A gap value of 0.73 meV was reported in the magnetron sputtering sample grown on thermally oxidized Si substrates [20]. A slightly larger gap of 0.83 meV was detected in PLD-grown TiN film [22]. Notably, the experiments using STS measurements revealed a clear spatial inhomogeneity with the gap values ranging from 0.2 to 1.1 meV [21]. Meanwhile, another typical nitride superconducting material, NbN, can also be used as a valuable reference. A complicated evolution of the gap ratio  $\Delta_0/k_B T_c$  (ranging from 1.95 to 2.22) with  $T_c$  and disorder level was uncovered in NbN films [36]. We sum-

TABLE III: Physical quantities calculated from the Hall and resistivity data.

Sample	$n$ $e/m^3$	$N(0)$ states/ $m^3 eV$	$\tau$ fs	$l$ nm	$k_F l$ —
Sapp-500	$7.1 \times 10^{28}$	$1.70 \times 10^{28}$	1.25	1.85	23.7
Si-500	$10.3 \times 10^{28}$	$1.92 \times 10^{28}$	1.95	3.28	47.6

marize these result in Table 2 to give a clear comparison with the present results.

Despite the significant divergence in experimental results regarding the SC of TiN thin films, there is still a lack of further investigation into the physical origin behind it. Especially, the underlying reasons for this change in coupling strength are worth exploring in depth. We first examined the lattice parameter changes caused by changes in substrate and growth temperature, which directly affect the electronic structure of the material. As we have stated, the lattice parameter is very close among the three samples with the relative variation below 0.5%. Thus we argue that change in lattice structure is unlikely to be the main factor causing differences in the coupling strength.

We know that disorder has a significant impact on superconductivity in low dimensional superconducting materials. On the one hand, strong disorder weakens the electron screening effect in the system, thereby reducing the value of SC gap [30]. On the other hand, disorder

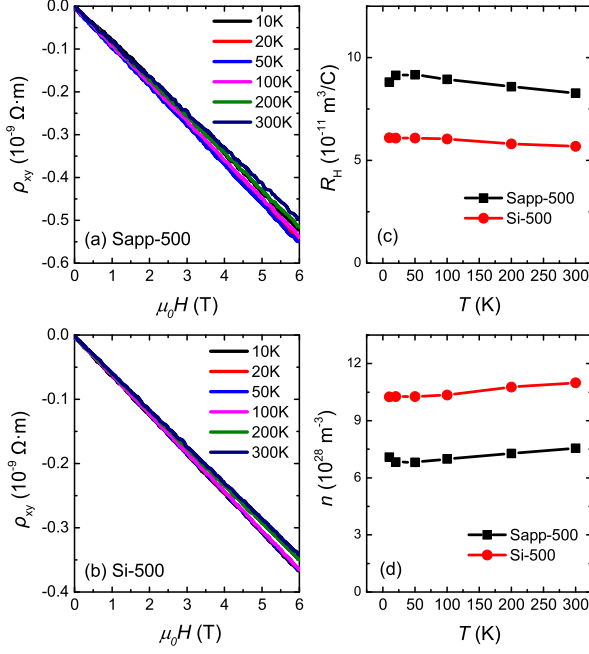


FIG. 5: Hall resistivity as a function of magnetic field of samples Sapp-500 (a) and Si-500 (b). Temperature dependence of Hall coefficient (c) and charge carrier density (d) of the two samples.

can lead to electron localization, which thereby reduces the density of states at the Fermi level  $N(0)$ . Actually, the data of  $\rho_n$  and RRR in Fig. 2 have shown some information concerning the disorder levels. To further check these two factors, we carried out Hall effect measurements on samples Sapp-500 and Si-500. As shown in Figs. 5(a) and (b), both samples reveal the linear behavior of the Hall resistivity  $\rho_{xy}$  versus magnetic field. Moreover, temperature has a rather weak effect on the Hall data. The Hall coefficient  $R_H$  and charge carrier density  $n$  are calculated from the Hall resistivity data, which are displayed in Figs. 5(c) and (d) respectively. One can see that the charge carrier density of sample Si-500 is about 50% higher than that of Sapp-50. Assuming a spherical Fermi surface, the values of  $N(0)$  can be derived to be  $1.70 \times 10^{28}$  and  $1.92 \times 10^{28}$  states/ $m^3$  eV from the Hall data at 10 K for the two samples respectively. Moreover, the relaxation time  $\tau$  and mean free path  $l$  of electron scattering have also been calculated combined with the resistivity data. The physical quantities calculated from the Hall and resistivity data are summarized in Table 3. The level of disorder is typically characterized by the Ioffe-Regel parameter  $k_F l$  [36], where  $k_F$  is the Fermi wave vector. It can be seen that compared to sample Si-500, sample Sapp-500 does indeed exhibit a substantially higher level of disorder. Meanwhile, the density of states at the Fermi level of sample Si-500 is higher than that of Sapp-500.

Although the increase in density of states and the decrease in disorder can qualitatively explain the strong-coupling feature exhibited in TiN films on Si substrates, comparisons with other systems can provide more clues. According to the previous report [36], the gap ratio  $\Delta_0/k_B T_c$  of NbN system reveals a mild increasing with the disorder levels  $k_F l \geq 2.3$ . At the same time, the values of  $N(0)$  and  $k_F l$  display a greater increase [37] compared to the that between Sapp-500 and Si-500 studied in this work. In other words, in the present TiN system, small changes in density of states and disorder are accompanied by a significant increase in energy gaps. In addition, it is notable that, compared with the NbN system with  $k_F l < 10$ , the present TiN films locate in a range with a lower level of disorder. Thus other factors, such as substrate changes and accompanying differences in crystal orientation, may also play important roles. Regarding this aspect, it is currently not entirely clear and deserves further in-depth research.

## CONCLUSIONS

Superconducting properties are investigated in TiN films grown on two different substrates. The superconducting critical temperature, normal-state resistivity and upper critical field all reveal a systematically evolution with the disorder level. Strikingly, the system undergoes a transition from weak coupling ( $\Delta_0/k_B T_c = 1.60 \sim 1.75$ ) to strong coupling ( $\Delta_0/k_B T_c = 3.05$ ), accompanied by a change in film orientation from (111) to (100), as the substrate changes from sapphire to Si. Further analysis indicates that this change in superconducting coupling strength is closely related to the difference in Coulomb screening effect caused by disorder and the change in density of states at the Fermi level.

## DATA AVAILABILITY STATEMENT

All data that support the findings of this study are included within the article.

## ACKNOWLEDGMENTS

This work is supported by the Shanghai Technology Innovation Action Plan Integrated Circuit Technology Support Program (Grant No. 22DZ1100200), and the National Key Research and Development Program of China (Grant No. 2023YFB4404904). The authors would like to thank all the staff at the Superconducting Electronics Facility (SELF) for their assistance.

---

\* wuyu@mail.sim.ac.cn

† mugang@mail.sim.ac.cn

‡ zrlin@mail.sim.ac.cn

- [1] W. Zhang, L. Y. You, H. Li, J. Huang, C. Lv, L. Zhang, X. Liu, J. Wu, Z. Wang, and X. Xie, *Sci. China-Phys. Mech. Astron.* **60**, 120314 (2017).
- [2] Q. Liu, H. Wang, Q. Zhang, J. Ren, W. Peng, and Z. Wang, *IEEE T. Appl. Supercon.* **27**, 1 (2017).
- [3] R. S. Shaikhaidarov, K. H. Kim1, J. W. Dunstan, I. V. Antonov, S. Linzen, M. Ziegler, D. S. Golubev, V. N. Antonov, E. V. Il'ichev, and Q. V. Astafiev, *Nature* **608**, 45 (2022).
- [4] X. Wang, Z. Xu, X. Liu, F. Xu, Y. Liu, W. Gao, Y. Wu, M. Yang, W. Peng, Z. Wang, et al., *Supercond. Sci. Technol.* **37**, 045001 (2024).
- [5] M. R. Vissers, J. Gao, D. S. Wisbey, D. A. Hite, C. C. Tsuei, A. D. Corcoles, M. Steffen, and D. P. Pappas, *Appl. Phys. Lett.* **97**, 232509 (2010).
- [6] P. Diener, H. Schellevis, and J. J. A. Baselmans, *Applied Physics Letters* **101**, 252601 (2012).
- [7] J. B. Chang, M. R. Vissers, A. D. Córcoles, M. Sandberg, J. Gao, D. W. Abraham, J. M. Chow, J. M. Gambetta, M. Beth Rothwell, G. A. Keefe, et al., *Appl. Phys. Lett.* **103**, 012602 (2013).
- [8] H. M. I. Jaim, J. A. Aguilar, B. Sarabi, Y. J. Rosen, A. N. Ramanayaka, E. H. Lock, C. J. K. Richardson, and K. D. Osborn, *IEEE Transactions on Applied Superconductivity* **25**, 1 (2015).
- [9] A. Torgovkin, S. Chaudhuri, A. Ruhtinas, M. Lahtinen, T. Sajavaara, and I. J. Maasilta, *Supercond. Sci. Technol.* **31**, 055017 (2018).
- [10] A. Shearrow, G. Koolstra, S. J. Whiteley, N. Earnest, P. S. Barry, F. J. Heremans, D. D. Awschalom, E. Shirokoff, and D. I. Schuster, *Applied Physics Letters* **113**, 212601 (2018).
- [11] R. Gao, W. Yu, H. Deng, H.-S. Ku, Z. Li, M. Wang, X. Miao, Y. Lin, and C. Deng, *Phys. Rev. Mater.* **6**, 036202 (2022).
- [12] B. O. Johansson, J. Sundgren, J. E. Greene, A. Rockett, and S. A. Barnett, *J. Vac. Sci. Technol. A* **3**, 303 (1985).
- [13] J. Narayan, P. Tiwari, X. Chen, J. Singh, R. Chowdhury, and T. Zheleva, *Applied Physics Letters* **61**, 1290 (1992).
- [14] R. Vispute, V. Talyansky, R. Sharma, S. Choopun, M. Downes, T. Venkatesan, Y. Li, L. Salamanca-Riba, A. Iliadis, K. Jones, et al., *Applied Surface Science* **127-129**, 431 (1998).
- [15] Y. Krockenberger, S.-i. Karimoto, H. Yamamoto, and K. Semba, *J. Appl. Phys.* **112**, 083920 (2012).
- [16] N. Hadacek, M. Sanquer, and J.-C. Villégier, *Phys. Rev. B* **69**, 024505 (2004).
- [17] T. I. Baturina, D. R. Islamov, J. Bentner, C. Strunk, M. R. Baklanov, and A. Satta, *Journal of Experimental and Theoretical Physics Letters* **79**, 337 (2004).
- [18] A. Mironov, T. Baturina, V. Vinokur, S. Postolova, P. Kropotin, M. Baklanov, D. Nasimov, and A. Latyshev, *Physica C* **470**, S808 (2010).
- [19] S. Gupta, A. Moatti, A. Bhaumik, R. Sachan, and J. Narayan, *Acta Materialia* **166**, 221 (2019).
- [20] W. Escoffier, C. Chapelier, N. Hadacek, and J.-C. Villégier, *Phys. Rev. Lett.* **93**, 217005 (2004).
- [21] W.-T. Liao, T. P. Kohler, K. D. Osborn, R. E. Butera, C. J. Lobb, F. C. Wellstood, and M. Dreyer, *Phys. Rev. B* **100**, 214505 (2019).
- [22] A. Torgovkin, A. Ruhtinas, and I. J. Maasilta, *IEEE Transactions on Applied Superconductivity* **31**, 1 (2021).
- [23] S. L. Prischepa, V. N. Kushnir, C. Cirillo, V. Granata, I. V. Komissarov, N. G. Kovalchuk, M. M. Mikhailik, A. L. Danilyuk, I. A. Svito, M. Andrulevičius, et al., *Supercond. Sci. Technol.* **34**, 115021 (2021).
- [24] A. V. Pogrebnyakov, J. M. Redwing, S. Raghavan, V. Vaithyanathan, D. G. Schlom, S. Y. Xu, Q. Li, D. A. Tenne, A. Soukiassian, X. X. Xi, et al., *Phys. Rev. Lett.* **93**, 147006 (2004).
- [25] Q.-Y. Wang, Z. Li, W.-H. Zhang, Z.-C. Zhang, J.-S. Zhang, W. Li, H. Ding, Y.-B. Ou, P. Deng, K. Chang, et al., *Chin. Phys. Lett.* **29**, 037402 (2012).
- [26] D. Jiang, B. Chen, Y. Liu, W. Peng, W. Li, Z. An, and G. Mu, *Supercond. Sci. Technol.* **37**, 035008 (2024).
- [27] D. Rasic, R. Sachan, M. F. Chisholm, J. Prater, and J. Narayan, *Cryst. Growth Des.* **17**, 6634 (2017).
- [28] N. Saveskul, N. Titova, E. Baeva, A. Semenov, A. Lubenchenko, S. Saha, H. Reddy, S. Bogdanov, E. Marinero, V. Shalaev, et al., *Phys. Rev. Appl.* **12**, 054001 (2019).
- [29] W.-P. Guo, R. Mishra, C.-W. Cheng, B.-H. Wu, L.-J. Chen, M.-T. Lin, and S. Gwo, *ACS Photonics* **6**, 1848 (2019).
- [30] P. W. Anderson, K. A. Muttalib, and T. V. Ramakrishnan, *Phys. Rev. B* **28**, 117 (1983).
- [31] Y. F. Wu, A. B. Yu, L. B. Lei, C. Zhang, T. Wang, Y. H. Ma, Z. Huang, L. X. Chen, Y. S. Liu, C. M. Schneider, et al., *Phys. Rev. B* **101**, 174502 (2020).
- [32] Y. Liu, H. Zhang, X. Han, T. Wang, L. Wang, Z. Niu, J. Pan, Z. Lin, W. Peng, Z. Li, et al., *Supercond. Sci. Technol.* **35**, 055010 (2022).
- [33] X. Wang, L. Wang, Y. Liu, W. Gao, Y. Wu, Z. Xu, H. Jin, L. Zhang, W. Peng, Z. Wang, et al., *Physica C* **606**, 1354223 (2023).
- [34] J. E. Jaffe, *Phys. Rev. B* **40**, 2558 (1989).
- [35] G. E. Blonder, M. Tinkham, and T. M. Klapwijk, *Phys. Rev. B* **25**, 4515 (1982).
- [36] S. P. Chockalingam, M. Chand, A. Kamlapure, J. Jesudasan, A. Mishra, V. Tripathi, and P. Raychaudhuri, *Phys. Rev. B* **79**, 094509 (2009).
- [37] S. P. Chockalingam, M. Chand, J. Jesudasan, V. Tripathi, and P. Raychaudhuri, *Phys. Rev. B* **77**, 214503 (2008).